Letter

High-Order Qubit Dephasing at Sweet Spots by Non-Gaussian Fluctuators: Symmetry Breaking and Floquet Protection

Ziwen Huang,* Xinyuan You, Ugur Alyanak, Alexander Romanenko, Anna Grassellino, and Shaojiang Zhu†

Superconducting Quantum Materials and Systems Center, Fermi National Accelerator Laboratory (FNAL), Batavia, Illinois 60510, USA

(Received 17 June 2022; revised 20 October 2022; accepted 25 October 2022; published 2 December 2022)

Although the Gaussian noise assumption is widely adopted in studying qubit decoherence, non-Gaussian noise sources have been detected in many qubits. Further understanding and mitigating the distinctive decoherence effect of the non-Gaussian noise remain critical. Here, we study the qubit dephasing caused by non-Gaussian fluctuators, and predict a symmetry-breaking effect that is unique to non-Gaussian noise. This broken symmetry results in an experimentally measurable mismatch between the extremum points of the dephasing rate and qubit frequency, which demands extra carefulness in characterizing the noise and locating the optimal working point. To further enhance the coherence time, we propose suppressing the second-order derivative of the qubit frequency by Floquet engineering. Our simulation on a tunable and gapped two-level quantum system, with the parameters from a heavy fluxonium, shows an order-of-magnitude improvement of the dephasing time, even after including the drive noise.

DOI: 10.1103/PhysRevApplied.18.L061001

Introduction.—Efficient quantum computing relies on high-coherence qubits and high-fidelity quantum operations [1,2]. However, further enhancement of the coherence times and gate fidelities toward full quantum error correction, one prerequisite for quantum computation [1–4], has been set back by decoherence [4–7]. Many solid-state qubits, for example superconducting qubits, are especially subject to uncontrolled low-frequency environmental fluctuations [5–33], such as the notorious $1/f$ noise [18–33].

This challenge has motivated research efforts on identifying, understanding, and mitigating the contributing noise channels [5–67]. Theoretically, noise is usually assumed as Gaussian, while realistic noise is more complicated. For example, if strong discrete fluctuators are present [13–18], the decoherence process of the qubits deviates significantly from prediction by assuming only Gaussian noise [5,8,9,13,27,38,39,44,45].

In this Letter, we focus on the special dephasing feature in qubits operated at sweet spots, where many flagship solid-state qubits reach their maximal dephasing time [23,26,31,52,55,62,63,67,68]. We report that non-Gaussian noise introduces a previously unrevealed dephasing feature, $\mathbb{Z}_2$ symmetry breaking. The breaking is predicted to cause an otherwise unexpected mismatch between the extremum points of the qubit dephasing rate and its oscillating frequency. Using a realistic non-Gaussian noise assumption, strong two-level fluctuators (TLFs), we demonstrate such mismatch in a concrete qubit model using two independent theoretical approaches. This finding provides a simple yet decisive tool to identify the non-Gaussian component in the noise background [53]. To further enhance the sweet-spot coherence time limited by such fluctuators (also Gaussian noise), we propose a triple-protection scheme via Floquet engineering [48,49,69–71], where the qubit is protected not only from dc fluctuation to the second order, but also from ac fluctuation to the first order.

Model.—The system we study is a tunable qubit subjected to low-frequency fluctuation. The full Hamiltonian under consideration is given by $\hat{H} = \hat{H}_q(\lambda) + \delta\xi(t)\hat{x}$, where $\hat{H}_q(\lambda)$ denotes the bare qubit Hamiltonian, $\delta\xi(t)$ describes the environmental fluctuation, and $\hat{x}$ is the operator to which the fluctuators are coupled. The qubit is tuned by an external control parameter λ according to $\hat{H}_q(\lambda) = \hat{H}_q(0) + \lambda\hat{x}$, which for example corresponds to the flux (charge) control of the fluxonium qubit (Cooper-pair box) [35,58]. We assume that the first-order derivative of this qubit vanishes at $\lambda = 0$, which is a result of a $\mathbb{Z}_2$ symmetry. Specifically, the Hamiltonian satisfies $\hat{R}\hat{H}_q(0)\hat{R}^\dagger = \hat{H}_q(0)$, where $\hat{R}$ is a reflection operation defined by the relation $\hat{R}\hat{x}\hat{R}^\dagger = -\hat{x}$. This symmetry ensures $(\partial\omega_j^{\text{bare}}/\partial\lambda)|_{\lambda=0} = 0$, where ω_j^{bare} is the eigenenergy of the jth eigenstate of the bare Hamiltonian $\hat{H}_q(\lambda)$. Note that the only specification

*zhuang@fnal.gov
†szhu26@fnal.gov

to such modeling is the existence of a symmetry-induced sweet spot, which extends our following discussion to a wide range of qubits exhibiting such working points [22,31,35,55,63,67]. For the noise $\delta\xi(t)$, we assume that the external control over the small range of λ under inspection only negligibly affects its properties.

$\mathbb{Z}_2$ symmetry and its breaking.—The symmetry we address is the invariance of the qubit density matrix elements, $\rho_{ij}(t)|_\lambda$, evaluated in their respective eigenbasis, under the reflection $\lambda \to -\lambda$. Such symmetry is strictly preserved if the fluctuation is Gaussian, and is generally broken for non-Gaussian $\delta\xi(t)$.

To rigorously derive the conclusion above, we first inspect the relation between the qubit Hamiltonians and eigenstates for $\pm\lambda$. The Hamiltonians are related by $\hat{H}_q(-\lambda) = \hat{R}\hat{H}_q(\lambda)\hat{R}^\dagger$, and the eigenstates can be conveniently chosen to satisfy $|j(-\lambda)\rangle = \hat{R}|j(\lambda)\rangle$. However, the interaction Hamiltonian $\hat{H}_I(t) \equiv \delta\xi(t)\hat{x}$ does not transform similarly due to the independence of $\hat{H}_I(t)$ on λ. This leads to a sign flipping of $\hat{H}_I(t)$ under reflection, i.e., $\hat{R}\hat{H}_I(t)\hat{R}^\dagger = -\hat{H}_I(t)$. As a result, the propagators transform as

$$\hat{R}\tilde{U}_I^\nu(t)|_\lambda\hat{R}^\dagger = (-1)^\nu\tilde{U}_I^\nu(t)|_{-\lambda}. \tag{1}$$

In the above equation, $\tilde{U}_I^\nu(t)$ is the νth-order term in the Dyson expansion of the interaction propagator $\tilde{U}_I(t) = \mathcal{T}\exp[-i\int_0^t dt'\tilde{H}_I(t')]$, where $\tilde{H}_I(t) = \hat{U}_0^\dagger(t)\hat{H}_I(t)\hat{U}_0(t)$ and $\hat{U}_0(t) \equiv \exp[-i\hat{H}_q(\lambda)t]$. The propagator $\tilde{U}_I(t)$ is expanded as $\tilde{U}_I(t) = \sum_\nu \tilde{U}_I^\nu(t)$, where $\tilde{U}_I^\nu(t)$ contains a product of ν times $\tilde{H}_I(t)$.

Crucially, sign flipping is further carried to the density matrix elements, which are expanded as

$$\begin{aligned}\rho_{I,jk}(t)|_\lambda &\equiv \overline{\langle j|\tilde{\rho}_I(t)|k\rangle}|_\lambda = \overline{\langle j|\tilde{U}_I(t)\tilde{\rho}_I(0)\tilde{U}_I^\dagger(t)|k\rangle}\Big|_\lambda \\ &= \sum_{j'k'\nu}\rho_{I,j'k'}(0)\,\Pi^\nu_{jk\leftarrow j'k'}(t)|_\lambda. \end{aligned}\tag{2}$$

Here, $\tilde{\rho}_I(t) = \hat{U}_0^\dagger(t)\hat{\rho}(t)\hat{U}_0(t)$ is the density matrix in the interaction picture and $\Pi^\nu_{jk\leftarrow j'k'}(t)|_\lambda$ is the νth order Keldysh projector. Using Eq. (1), we find $\Pi^\nu_{jk\leftarrow j'k'}(t)|_\lambda = (-1)^\nu\Pi^\nu_{jk\leftarrow j'k'}(t)|_{-\lambda}$, which implies that $\rho_{I,jk}(t)|_\lambda$ and $\rho_{I,jk}(t)|_{-\lambda}$ are unequal in general, unless all odd projectors are irrelevant. Gaussian noise ensures this condition due to its vanishing odd correlation functions, such as $\overline{\delta\xi_G(t)\delta\xi_G(t_1)\delta\xi_G(0)} = 0$, which leads to $\rho_{I,jk}(t)|_{-\lambda} = \rho_{I,jk}(t)|_\lambda$ given identical initial matrix elements (similarly for laboratory-frame matrices). On the other hand, non-Gaussian noise does not in general preserve this equality. We summarize the discussion of symmetry breaking and preserving in Fig. 1.

To theoretically confirm the predicted symmetry breaking, we adopt a simple yet realistic model, i.e., strong TLFs

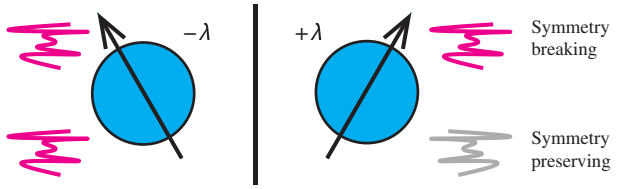

FIG. 1. A cartoon illustrating how noise breaks the reflection symmetry of a qubit. The noise term $\hat{H}_I(t)$ (bottom gray curve) remains invariant under the external operation $-\lambda \to \lambda$, which in general breaks the reflection symmetry, unless the statistical effect of $\delta\xi(t)$ is identical to that of $-\delta\xi(t)$.

[27,38,39]. This model is motivated by both the microscopic understanding of the materials used in solid-state qubits [5] and abundant experimental evidence [13–18]. To make our results more broadly applicable, the full fluctuation $\delta\xi(t)$ consists of both Gaussian noise and N_T strong TLFs, which specifies $\delta\xi(t) = \sum_{\mu=1}^{N_T}\delta\xi_{T\mu}(t) + \delta\xi_G(t)$. The TLFs can only take two values, i.e., $\pm|\xi_{T\mu}| - \bar{\xi}_{T\mu}$, where $|\xi_{T\mu}|$ describes the noise magnitude and $\bar{\xi}_{T\mu}$ is used to cancel the time average of the fluctuator.

The high-order dephasing rates contributed by these fluctuators are derived using the Keldysh diagrammatic technique [40,59,60,72,73]. It provides an expression of the free-induced (Ramsey) evolution of the off-diagonal matrix element $\rho_{eg}(t) \approx \rho_{eg}(0)\exp[-i\omega_q' t - \Phi(t)]$. Here, the Lamb-shifted qubit oscillation frequency is approximated by $\omega_q' \approx \Delta + D_{2,\lambda=0}\left[\lambda^2 + \int d\omega S(\omega)/2\pi\right]/2$, where the coefficient $D_{2,\lambda=0} \equiv (\partial^2\omega_{ge}^{\rm bare}/\partial\lambda^2)|_{\lambda=0}$ denotes the second-order derivative of the bare qubit frequency and Δ is the extremum qubit bare frequency, $\Delta \equiv (\omega_e^{\rm bare} - \omega_g^{\rm bare})|_{\lambda=0}$. (The integration limits in $\int_{-\infty}^{\infty}$ are omitted to save space.) The dephasing profile $\Phi(t)$ is divided into multiple contributions $\Phi(t) \approx \Phi_G(t) + \sum_{\mu=1}^{N_T}\Phi_{T\mu}(t) + \sum_{\upsilon\neq\upsilon'}\Phi_{\upsilon\upsilon'}(t)$, where $\Phi_G(t)$, $\Phi_{T\mu}(t)$, and $\Phi_{\upsilon\upsilon'}(t)$ are contributed by the Gaussian noise, the μth TLF, and mutual effect of two different components. Specifically, we find

$$\begin{aligned}\Phi_G(t) &= D_{2,\lambda=0}^2\lambda^2\int\frac{d\omega}{2\pi}S_G(\omega)K^R(\omega,t) \\ &\quad + \frac{D_{2,\lambda=0}^2}{2}\iint\frac{d\omega}{2\pi}\frac{d\omega'}{2\pi}S_G(\omega)S_G(\omega')K^R(\omega+\omega',t), \\ \Phi_{T\mu}(t) &= D_{2,\lambda=0}^2\left(\lambda - \bar{\xi}_{T\mu}\right)^2\int\frac{d\omega}{2\pi}S_{T\mu}(\omega)K^R(\omega,t), \\ \Phi_{\upsilon\upsilon'}(t) &= \frac{D_{2,\lambda=0}^2}{2}\iint\frac{d\omega}{2\pi}\frac{d\omega'}{2\pi}S_\upsilon(\omega)S_{\upsilon'}(\omega')K^R(\omega+\omega',t).\end{aligned}\tag{3}$$

In the above, $S_\upsilon(\omega)$ is the Fourier transformation of the two-point correlation functions, $S_\upsilon(\omega) = \int dt\,\overline{\xi_\upsilon(t)\xi_\upsilon(0)}e^{i\omega t}$ ($\upsilon = G, T\mu$ and $\mu = 1,2,\ldots,N_T$), and the sum spectrum

is denoted by $S(\omega) = \sum_\upsilon S_\upsilon(\omega)$. These spectra are sampled time-dependently according to the filter function $K^R(\omega, t) \equiv t^2 \mathrm{sinc}^2(\omega t/2)/2$. In Eq. (3), $\Phi_{\mathcal{T}\mu}(t)$ does not preserve the $\mathbb{Z}_2$ symmetry, since nonzero $\bar{\xi}_{\mathcal{T}\mu}$ leads to $\Phi_{\mathcal{T}\mu}(t)|_\lambda \neq \Phi_{\mathcal{T}\mu}(t)|_{-\lambda}$. Meanwhile, up to leading order, the Lamb-shifted qubit frequency is still symmetric, implying an unexpected mismatch between the extremum points of the dephasing rate and frequency.

In addition to the analytical calculation, we further confirm our prediction independently using the stochastic Schrödinger equation (SSE) [38,39]. This method averages the ensemble of traces of the qubit evolution according to many realizations of the random fluctuation. We choose to simulate the heavy fluxonium qubit as a concrete example, which can be approximated by a tunable and gapped two-level quantum system, as $\hat{H}_q(\lambda) \approx \Delta\hat{\sigma}_x/2 + \lambda C_\phi \hat{\sigma}_z/2$ [26,48] (C_ϕ is an unimportant coefficient). This simple model renders the SSE results also qualitatively applicable to other widely used tunable qubits [22,31,52,63,67]. The fluctuation used in this simulation is generated according to $\delta\xi(t) = \sum_{\mu=1}^{N_T} \delta\xi_{\mathcal{T}\mu}(t) + \delta\xi_G(t)$.

In Figs. 2(a) and 2(b), we plot the calculated qubit frequencies and dephasing rates as functions of the control parameter λ for $N_T = 0$ (purely Gaussian) and 1 (non-Gaussian), respectively. Both the dephasing rates γ_2 and the qubit frequency ω_q' are extracted by fitting the simulated Ramsey measurement using a simple exponential function over the same time range. (Note that the dephasing profile is not exactly exponential given the structured noise we use, and this simplest protocol is only chosen for consistency in comparing the simulation results.) For both cases, we find impressive agreement between our analytical prediction (dashed lines) and numerical simulation (squares). In Fig. 2(a), the Gaussian fluctuator $\delta\xi_G(t)$ ensures the $\mathbb{Z}_2$ symmetry under the reflection $-\lambda \to \lambda$. In Fig. 2(b), we observe a measurable mismatch between the minimum points of the dephasing rate and the qubit frequency. For a more intuitive demonstration of such mismatch, we showcase two simulated Ramsey signals in Fig. 2(c), taken at the minimum points of the dephasing rate (red star) and qubit frequency (blue star) in Fig. 2(b). Although the red signal decays slower, it oscillates faster compared with the blue one. This mismatch demands more carefulness in locating the optimal working point experimentally: the extremum point of the qubit frequency is not necessarily the qubit dephasing sweet spot. Our simulation shows that the Ramsey dephasing rates at the two mismatched minimum points differ by a factor of 2. Note that in disagreement with the Keldysh prediction, the SSE results also show a shift of the minimum of the qubit frequency from $\lambda = 0$ for the non-Gaussian case. We attribute this to the lower accuracy of the perturbation theory at long times ($t \sim 0.5$ ms). [Much better agreement is found for the fitting over $0 < t < 20$ μs, as plotted by light pink circles in Fig. 2(b).]

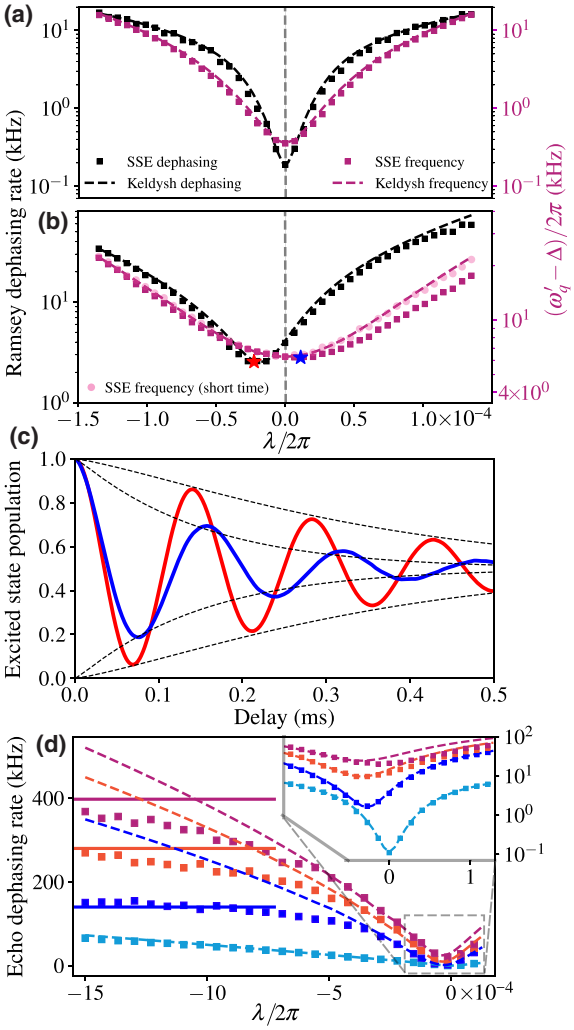

FIG. 2. Noise-mediated evolutions of a tunable qubit around its sweet spot. (a),(b) The calculated qubit frequency (purple) and dephasing rates (black) by the Keldysh perturbation theory (dashed lines) and SSE (squares and dots) by simulating Ramsey measurements. (c) The red and blue curves are the simulated Ramsey signals at the points marked by red and blue stars in (b), respectively. The black dashed curves describe the dephasing profile predicted using Eq. (3). We choose $N_T = 0$ for (a) and $N_T = 1$ for (b),(c). (d) The fitted Echo dephasing rates over a wider range of control parameters, where the dashed curves are from analytical calculation and the squares from SSE. The number of TLFs N_T is varied from 0 to 3 (cyan, blue, red, purple). The solid lines mark the projected saturation rates. The simulated qubit is a heavy fluxonium qubit, with parameters from Ref. [26]. The sweet spot is located at $\phi_{\mathrm{ext}} = \pi$, rendering $\lambda = \phi_{\mathrm{ext}} - \pi$ and $\hat{x} \equiv E_L\hat{\varphi}$. The strong TLFs have a magnitude $|\xi_T|/2\pi = 9 \times 10^{-5}$ and uneven probability distribution $P_{-(+)} = 0.7(0.3)$. The Gaussian noise is approximated by 2001 weak and independent TLFs, which have a $1/\kappa$ distribution [47,64] to mimic the $1/f$ noise ($\kappa \in [1\,\mathrm{kHz}, 1\,\mathrm{MHz}]$, $|\delta\xi_G(t)|/2\pi = 2 \times 10^{-5}$).

Farther away from the sweet spot, the dephasing rates are also constantly measured for the characterization of the low-frequency noise [23,26,30,55]. In this operating region, the non-Gaussian noise also dephases the qubit

distinctively from its Gaussian counterpart [38,39,42,44,45]. To reveal the difference in detail, we use the analytical (dashed lines) and numerical (squares) methods to simulate the dephasing rates in this parameter region. We plot the results in Fig. 2(d). (We switch to the Echo protocol to avoid complicated beatings.) In the presence of strong TLFs, the dephasing rate contributed by the TLFs saturates toward larger $|\lambda|$ [38,39,42,45]. The saturated dephasing rates are derived as $\overline{\kappa} = \sum_{\vec{\eta}} \overline{\kappa}_{\vec{\eta}} P_{\vec{\eta}}$ [73], where $\vec{\eta}$ is one configuration of the group of strong TLFs, and $\kappa_{\vec{\eta}}$ and $P_{\vec{\eta}}$ are the corresponding flipping rate and probability. These predicted saturation rates (solid lines) well capture the behaviors of the dephasing rates at the far left part of the Fig. 2(d). Such saturation behavior, which is beyond the description of the Gaussian noise model, cautions the use of the Gaussian noise assumption in noise characterization.

Triple protection by floquet engineering.—Our calculations point out the crucial role of the second-order derivative $D_{2,\lambda=0}$ in limiting the optimal coherence times, for the presence of both Gaussian noise and non-Gaussian TLFs. To further enhance the coherence time (while maintaining the qubit controllability), it is ideal to design a qubit with a flatter spectrum [35,36,50,55,66]. However, the experimental implementation of some of these qubits for their full protection encounters challenges from the experimental limits on the circuit parameters [7,55]. In the following, we present a drive-based protocol to suppress the second-order sensitivity [74], which can circumvent the hardware limitations.

This protocol is based on the Floquet-engineering techniques developed in Refs. [48,49], while here we require not only the first-order insensitivity $\partial\varepsilon_{01}/\partial\lambda = 0$, but also the second order $\partial^2\varepsilon_{01}/\partial^2\lambda = 0$ (ε_{01} denotes the *bare* quasienergy difference). In addition to these requirements, it is also crucial to ensure the insensitivity of the qubit to the drive noise, since Refs. [49,51,52,61,65,75] point out that the fluctuation of the drive amplitude also causes qubit dephasing. Therefore, the optimal protection scheme should also include $\partial\varepsilon_{01}/\partial A = 0$, where A denotes the drive amplitude. The operating points where the three aforementioned derivatives vanish are referred to as the *triple sweet spots*. Using the two-level approximated qubit model again, we find that these points can be obtained by driving the qubit with $\hat{H}_d(t) = A[\cos\omega_d t + \alpha\cos(2n+1)\omega_d t]\hat{x}$ ($n \in \mathbb{N}^+$). (We choose an odd integer $2n+1$ to ensure the vanishing of $\partial\epsilon_{01}/\partial\lambda$ [73].) This driving protocol is also used in Refs. [51,52], although an extra second-order protection is targeted. The position of one triple sweet spot is shown in Fig. 3(a), where we choose $\alpha = 1$ and $n = 1$. In Fig. 3(b), we plot the quasienergies of the qubit as a function of the dc control parameter λ, with the ac drive amplitude A fixed at the sweet spot, and the other way around in Fig. 3(c). Both plots show suppressed variation of the qubit frequency around the sweet spot. In Fig. 3(b), the variation of the frequency of the undriven qubit (subtracted by integer multiples of the drive frequency for comparison) is plotted (red-dashed curve) to contrast the second-order suppression. According to Eq. (3), this protection protocol should mitigate dephasing caused by both the Gaussian noise and the non-Gaussian TLFs.

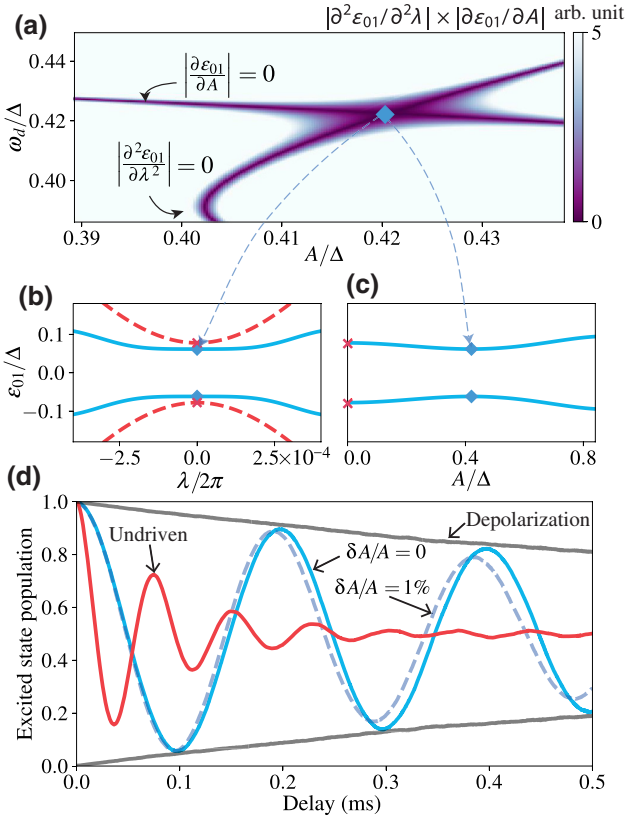

FIG. 3. Floquet engineering of the triple sweet spots. (a) Plots the product of the derivatives, i.e., $|\partial\varepsilon_{01}^2/\partial\lambda^2| \times |\partial\varepsilon_{01}/\partial A|$. The crossing of the two dark curves hosts the triple sweet spot (cyan diamond). The quasienergy spectra as functions of (b) the dc control parameter λ and (c) the drive amplitude A. The red dashed lines describe the quasienergies of the undriven bare fluxonium and the crosses mark the location of static working points ($A = 0$). (d) Comparison of the simulated Ramsey measurements between the Floquet-engineered triple sweet spot (cyan) and the static one (red). The simulation shown by the dashed cyan curve includes 1% random fluctuation in A, and the solid gray curves describe the Floquet depolarization.

The discussion above only assumes a tunable two-level quantum system. To quantitatively confirm the improved coherence times by SSE, we again take the heavy fluxonium as an example to simulate the Floquet Ramsey evolution [49]. The dephasing time is compared with that in the undriven case in Fig. 3(d). Using the same noise model $\delta\xi(t)$ ($N_T = 2$ for this simulation), the dephasing time at this triple protection point (solid cyan curve) is improved by 10 times compared with that at the static sweet spot (solid red curve). This is directly related to the suppression of the second-order derivative [Fig. 3(b)].

The limiting factor for the coherence time at this protection point is the depolarization (solid gray curves) by the noise at the smaller qubit frequency, which can potentially be further mitigated by optimizing the qubit parameters and drive shapes. To emulate the low-frequency drive noise, we further include random fluctuation of the drive amplitude A before each SSE trace. Remarkably, we still find 8 times improvement (cyan dashed curve) for up to 1% of such fluctuation. This experimentally appreciable robustness is owing to the first-order insensitivity of the quasienergy difference to the drive amplitude [Fig. 3(c)].

Conclusion.—We study the high-order dephasing effect in a qubit by non-Gaussian fluctuators. Our calculation predicts a symmetry breaking that is unique to the non-Gaussian noise. Concretely, strong TLFs dramatically change the behavior of the dephasing rates and cause an unexpected mismatch between the minimum points of the dephasing rate and the qubit frequency. These findings challenge the usually assumed equivalence between the two minimum points, call for extra carefulness in locating the optimal working point, and caution the use of the Gaussian model for noise characterization. Finally, we propose a triple-protection scheme to suppress the second-order sensitivity of the qubit energy to these fluctuators, where the qubit is also first-order protected from the low-frequency drive noise. The enhancement of an order of magnitude in dephasing time is numerically confirmed. Such enhancement is fully compatible with qubit control and scalability [48,70,71], making the triple-protection technique a powerful tool toward large-scale and noise-resilient quantum computation.

Acknowledgments.—This material is based upon work supported by the U.S. Department of Energy, Office of Science, National Quantum Information Science Research Centers, Superconducting Quantum Materials and Systems Center (SQMS) under Contract No. DE-AC02-07CH11359. We thank Jens Koch, David I. Schuster, András Gyenis, Peter Groszkowski, Wei-Ting Lin, Pranav S. Mundada, and Helin Zhang for constructive discussions.

[1] D. P. DiVincenzo, The physical implementation of quantum computation, Fortschr. Phys. **48**, 771 (2000).
[2] J. Preskill, Quantum computing in the NISQ era and beyond, Quantum **2**, 79 (2018).
[3] M. Kjaergaard *et al.*, Superconducting qubits: Current state of play, Annu. Rev. Condens. Matter Phys. **11**, 369 (2020).
[4] C. D. Bruzewicz *et al.*, Trapped-ion quantum computing: Progress and challenges, Appl. Phys. Rev. **6**, 021314 (2019).
[5] C. Müller *et al.*, Towards understanding two-level-systems in amorphous solids: Insights from quantum circuits, Rep. Prog. Phys. **82**, 124501 (2019).
[6] C. E. Murray, Material matters in superconducting qubits, Mater. Sci. Eng. R Rep. **146**, 100646 (2021).
[7] A. Gyenis *et al.*, Moving Beyond the Transmon: Noise-Protected Superconducting Quantum Circuits, PRX Quantum **2**, 030101 (2021).
[8] P. Dutta and P. M. Horn, Low-frequency fluctuations in solids: $\frac{1}{f}$ noise, Rev. Mod. Phys. **53**, 497 (1981).
[9] M. B. Weissman, $\frac{1}{f}$ noise and other slow, nonexponential kinetics in condensed matter, Rev. Mod. Phys. **60**, 537 (1988).
[10] P. Kumar *et al.*, Origin and Reduction of $1/f$ Magnetic Flux Noise in Superconducting Devices, Phys. Rev. Appl. **6**, 041001 (2016).
[11] K. Serniak *et al.*, Hot Nonequilibrium Quasiparticles in Transmon Qubits, Phys. Rev. Lett. **121**, 157701 (2018).
[12] M. Constantin and C. C. Yu, Microscopic Model of Critical Current Noise in Josephson Junctions, Phys. Rev. Lett. **99**, 207001 (2007).
[13] S. Schlör *et al.*, Correlating Decoherence in Transmon Qubits: Low Frequency Noise by Single Fluctuators, Phys. Rev. Lett. **123**, 190502 (2019).
[14] D. Rieger *et al.*, Gralmonium: Granular aluminum nanojunction fluxonium qubit, arXiv:2202.01776.
[15] V. Zaretskey *et al.*, Spectroscopy of a Cooper-pair box coupled to a two-level system via charge and critical current, Phys. Rev. B **87**, 174522 (2013).
[16] J. Lisenfeld *et al.*, Observation of directly interacting coherent two-level systems in an amorphous material, Nat. Commun. **6**, 6182 (2015).
[17] J. H. Béjanin *et al.*, Interacting defects generate stochastic fluctuations in superconducting qubits, Phys. Rev. B **104**, 094106 (2021).
[18] T. McCourt *et al.*, Learning noise via dynamical decoupling of entangled qubits, arXiv:2201.11173.
[19] R. C. Bialczak *et al.*, $1/f$ Flux Noise in Josephson Phase Qubits, Phys. Rev. Lett. **99**, 187006 (2007).
[20] D. Vion *et al.*, Manipulating the quantum state of an electrical circuit, Science **296**, 886 (2002).
[21] Y. Nakamura *et al.*, Coherent control of macroscopic quantum states in a single-Cooper-pair box, Nature **398**, 786 (1999).
[22] Y. Nakamura *et al.*, Charge Echo in a Cooper-Pair Box, Phys. Rev. Lett. **88**, 047901 (2002).
[23] L. B. Nguyen *et al.*, High-Coherence Fluxonium Qubit, Phys. Rev. X **9**, 041041 (2019).
[24] Y.-H. Lin *et al.*, Demonstration of Protection of a Superconducting Qubit from Energy Decay, Phys. Rev. Lett. **120**, 150503 (2018).
[25] N. Earnest *et al.*, Realization of a Λ System with Metastable States of a Capacitively Shunted Fluxonium, Phys. Rev. Lett. **120**, 150504 (2018).
[26] H. Zhang *et al.*, Universal Fast-Flux Control of a Coherent, Low-Frequency Qubit, Phys. Rev. X **11**, 011010 (2021).
[27] E. Paladino *et al.*, $1/f$ noise: Implications for solid-state quantum information, Rev. Mod. Phys. **86**, 361 (2014).
[28] I. Chiorescu *et al.*, Coherent quantum dynamics of a superconducting flux qubit, Science **299**, 1869 (2003).
[29] C. M. Quintana *et al.*, Observation of Classical-Quantum Crossover of $1/f$ Flux Noise and Its Paramagnetic Temperature Dependence, Phys. Rev. Lett. **118**, 057702 (2017).
[30] J. Braumüller *et al.*, Characterizing and Optimizing Qubit Coherence Based on SQUID Geometry, Phys. Rev. Appl. **13**, 054079 (2020).

[31] F. Yan *et al.*, The flux qubit revisited to enhance coherence and reproducibility, Nat. Commun. **7**, 12964 (2016).

[32] D. Kim *et al.*, Microwave-driven coherent operation of a semiconductor quantum dot charge qubit, Nat. Nano **10**, 243 (2015).

[33] B. Thorgrimsson *et al.*, Extending the coherence of a quantum dot hybrid qubit, Npj Quantum Inf. **3**, 32 (2017).

[34] G. Catelani *et al.*, Decoherence of superconducting qubits caused by quasiparticle tunneling, Phys. Rev. B **86**, 184514 (2012).

[35] J. Koch *et al.*, Charge-insensitive qubit design derived from the Cooper pair box, Phys. Rev. A **76**, 042319 (2007).

[36] P. Groszkowski *et al.*, Coherence properties of the 0-π qubit, New J. Phys. **20**, 043053 (2018).

[37] J. Schriefl *et al.*, Decoherence from ensembles of two-level fluctuators, New J. Phys. **8**, 1 (2006).

[38] G. Falci *et al.*, Initial Decoherence in Solid State Qubits, Phys. Rev. Lett. **94**, 167002 (2005).

[39] E. Paladino *et al.*, Decoherence and $1/f$ Noise in Josephson Qubits, Phys. Rev. Lett. **88**, 228304 (2002).

[40] Y. Makhlin and A. Shnirman, Dephasing of Solid-State Qubits at Optimal Points, Phys. Rev. Lett. **92**, 178301 (2004).

[41] T. Itakura and Y. Tokura, Dephasing due to background charge fluctuations, Phys. Rev. B **67**, 195320 (2003).

[42] J. Bergli *et al.*, Decoherence in qubits due to low-frequency noise, New J. Phys. **11**, 025002 (2009).

[43] M. A. C. Rossi and M. G. A. Paris, Non-Markovian dynamics of single- and two-qubit systems interacting with Gaussian and non-Gaussian fluctuating transverse environments, J. Chem. Phys. **144**, 024113 (2016).

[44] J. Bergli *et al.*, Decoherence of a qubit by non-Gaussian noise at an arbitrary working point, Phys. Rev. B **74**, 024509 (2006).

[45] Y. M. Galperin, B. L. Altshuler, J. Bergli, and D. V. Shantsev, Non-Gaussian Low-Frequency Noise as a Source of Qubit Decoherence, Phys. Rev. Lett. **96**, 097009 (2006).

[46] G. Ithier *et al.*, Decoherence in a superconducting quantum bit circuit, Phys. Rev. B **72**, 134519 (2005).

[47] X. You *et al.*, Positive- and negative-frequency noise from an ensemble of two-level fluctuators, Phys. Rev. Res. **3**, 013045 (2021).

[48] Z. Huang *et al.*, Engineering Dynamical Sweet Spots to Protect Qubits from $1/f$ Noise, Phys. Rev. Appl. **15**, 034065 (2021).

[49] P. S. Mundada *et al.*, Floquet-Engineered Enhancement of Coherence Times in a Driven Fluxonium Qubit, Phys. Rev. Appl. **14**, 054033 (2020).

[50] D. K. Weiss *et al.*, Spectrum and coherence properties of the current-mirror qubit, Phys. Rev. B **100**, 224507 (2019).

[51] N. Didier, Flux control of superconducting qubits at dynamical sweet spot, arXiv:1912.09416.

[52] J. A. Valery *et al.*, Dynamical Sweet Spot Engineering via Two-Tone Flux Modulation of Superconducting Qubits, PRX Quantum **3**, 020337 (2022).

[53] Y. Sung *et al.*, Non-Gaussian noise spectroscopy with a superconducting qubit sensor, Nat. Commun. **10**, 3715 (2019).

[54] J. Bylander *et al.*, Noise spectroscopy through dynamical decoupling with a superconducting flux qubit, Nat. Phys. **7**, 565 (2011).

[55] A. Gyenis *et al.*, Experimental Realization of a Protected Superconducting Circuit Derived from the 0-π Qubit, PRX Quantum **2**, 010339 (2021).

[56] A. P. M. Place *et al.*, New material platform for superconducting transmon qubits with coherence times exceeding 0.3 milliseconds, Nat. Commun. **12**, 1779 (2021).

[57] C. Wang *et al.*, Towards practical quantum computers: Transmon qubit with a lifetime approaching 0.5 milliseconds, npj Quantum Inf. **8**, 3 (2022).

[58] V. E. Manucharyan *et al.*, Fluxonium: Single Cooper-pair circuit free of charge offsets, Science **326**, 113 (2009).

[59] Y.-X. Wang and A. A. Clerk, Spectral characterization of non-Gaussian quantum noise: Keldysh approach and application to photon shot noise, Phys. Rev. Res. **2**, 033196 (2020).

[60] Y. Makhlin and A. Shnirman, Dephasing of qubits by transverse low-frequency noise, J. Exp. Theor. Phys. **78**, 497 (2003).

[61] S. S. Hong *et al.*, Demonstration of a parametrically activated entangling gate protected from flux noise, Phys. Rev. A **101**, 012302 (2020).

[62] A. Somoroff *et al.*, Millisecond coherence in a superconducting qubit, arXiv:2103.08578.

[63] K. Kalashnikov *et al.*, Bifluxon: Fluxon-Parity-Protected Superconducting Qubit, PRX Quantum **1**, 010307 (2020).

[64] A. Shnirman, G. Schön, I. Martin, and Y. Makhlin, Low- and High-Frequency Noise from Coherent Two-Level Systems, Phys. Rev. Lett. **94**, 127002 (2005).

[65] N. Didier *et al.*, Ac Flux Sweet Spots in Parametrically Modulated Superconducting Qubits, Phys. Rev. Appl. **12**, 054015 (2019).

[66] J. Q. You *et al.*, Low-decoherence flux qubit, Phys. Rev. B **75**, 140515 (2007).

[67] Y.-C. Yang, S. N. Coppersmith, and M. Friesen, Achieving high-fidelity single-qubit gates in a strongly driven charge qubit with 1/f charge noise, Npj Quantum Inf. **5**, 12 (2019).

[68] Q. Ficheux *et al.*, Fast Logic with Slow Qubits: Microwave-Activated Controlled-Z Gate on Low-Frequency Fluxoniums, Phys. Rev. X **11**, 021026 (2021).

[69] J. M. Pirkkalainen *et al.*, Hybrid circuit cavity quantum electrodynamics with a micromechanical resonator, Nature **494**, 211 (2013).

[70] A. Gandon *et al.*, Engineering, Control, and Longitudinal Readout of Floquet Qubits, Phys. Rev. Appl. **17**, 064006 (2022).

[71] A. Di Paolo *et al.*, Extensible aircuit-qed architecture via amplitude- and frequency-variable microwaves, arXiv:2204.08098.

[72] C. Müller and T. M. Stace, Deriving Lindblad master equations with Keldysh diagrams: Correlated gain and loss in higher order perturbation theory, Phys. Rev. A **95**, 013847 (2017).

[73] See Supplemental Material at http://link.aps.org/supplemental/10.1103/PhysRevApplied.18.L061001 for the analytical derivation of the dephasing profile of the qubit around its sweet spot for the static and driven cases.

[74] J. Picó-Cortés and G. Platero, Dynamical second-order noise sweetspots in resonantly driven spin qubits, Quantum **5**, 607 (2021).

[75] I. Cohen *et al.*, Continuous dynamical decoupling utilizing time-dependent detuning, Fortschr. Phys. **65**, 1600071 (2017).